

RTIC: Residual Learning for Text and Image Composition using Graph Convolutional Network

Minchul Shin, Yoonjae Cho, Byungsoo Ko, Geonmo Gu
NAVER/LINE Vision

{min.stellastra, yoonjae.cho92, kobiso62, korgm403}@gmail.com

Abstract

In this paper, we study the compositional learning of images and texts for image retrieval. The query is given in the form of an image and text that describes the desired modifications to the image; the goal is to retrieve the target image that satisfies the given modifications and resembles the query by composing information in both the text and image modalities. To accomplish this task, we propose a simple new architecture using skip connections that can effectively encode the errors between the source and target images in the latent space. Furthermore, we introduce a novel method that combines the graph convolutional network (GCN) with existing composition methods. We find that the combination consistently improves the performance in a plug-and-play manner. We perform thorough and exhaustive experiments on several widely used datasets, and achieve state-of-the-art scores on the task with our model. To ensure fairness in comparison, we suggest a strict standard for the evaluation because a small difference in the training conditions can significantly affect the final performance. We release our implementation, including that of all the compared methods, for reproducibility.

1. Introduction

Combining visual and contextual information, in which the desired items can be found not only from an image but also with a modification text that describes the desired modifications, enables search engines to provide users with a powerful and intuitive experience for visual search. Among the various approaches [30, 39, 1] that have been employed to solve this problem, *image-text composition* is considered as the most direct and intuitive approach. The main principle behind this approach is to learn a non-linear mapping from a pair comprising the source image and the modification text describing the target image, given the ground-truth triplet pairs. *Image-text composition* [2, 33, 29, 7, 6, 18] is a subset problem of *feature fusion* [4, 3, 21, 37, 38, 11],



Figure 1. Our concept for encoding relationships between the nodes which are defined as *image-text* pairs in the graph. we consider a group of green-bordered pairs is highly correlated with one another because the pairs in the group describe visually similar target images.

with the special constraint that the output representation is required to be embedded in the image feature space and not in an arbitrary space.

One challenge in *image-text composition* is data scarcity because collecting the ground-truth *image-text* pairs is extremely expensive. Therefore, it is inevitable that only a small amount of data is available for training, which causes the model to generalize poorly. To remedy this, we suggest a graph convolutional network (GCN)-based regularization technique that can be interpreted as a special form of semi-supervised learning. We explore the possibility of utilizing graph information that encodes the similarity between *image-text* pairs as shown in Figure 1. The proposed graph-based technique, named the GCN stream, can be attached to any existing composition method. We found that joint training with the GCN stream consistently improves the results of all existing methods in a plug-and-play manner.

In designing the composition module, we place special focus on the use of the skip connection [15] because of its powerful ability to learn representations. We found that little attention has been paid to this idea in the *image-text* com-

position task, despite its simplicity. In this paper, we propose a simple new architecture for composing an image and text based on skip connections. Our method can be considered as an advanced variant of TIRG [33] designed with careful consideration of the task.

While we experimentally show that our model can achieve state-of-the-art performance on the task, our ultimate goal is not to obtain the best score on the benchmark but to perform an objective comparison between composition methods under restricted conditions. The existing methods [2, 7, 6, 18] address not only the composition method itself but also various aspects of training (e.g., *the extraction of features and the definition of loss function*). Although such techniques significantly improve the score, the results are hardly reproducible and lead to unfair comparisons between the composition methods. Furthermore, we found that significant randomness in the score exists in this task, even between models trained with the same training parameters. This phenomenon makes it difficult to analyze the behavior of the models. Therefore, we address the need for a standard for training to ensure objectiveness and fairness in performing comparisons across papers.

Main contributions. In summary, the main contributions of our work are threefold: First, we introduce a simple but powerful *image-text composition* architecture, RTIC, that effectively uses skip connections for error encoding. Second, we propose using the GCN stream as a good regularizer, to improve the results of any existing method, which can be trained jointly in a plug-and-play manner. Finally, we suggest a baseline training standard that removes the uncertainty caused by different training conditions. We perform all our experiments based on this training standard and release our implementation, including that of all the compared methods, for future reproducibility.

2. Related Work

Image and Text Composition. Many studies [4, 3, 21, 37, 38, 11] have investigated effective ways to combine more than two different modalities in *feature fusion*. The *image and text composition* task is a subset problem of *feature fusion*. Increasing attention has recently been paid to this task due to the release of public datasets such as Fashion-IQ [14]. In their pioneering work, Vo *et al.* [33] proposed TIRG, which uses a gating mechanism to determine the channels of the image representation to be modified conditioned by a text. Based on their work, various methods [2, 33, 29, 7, 6, 18] that achieved state-of-the-art results on this task have been reported. VAL [7] employs a hierarchical feature matching that exploits the intermediate features from the image encoder. TRACE [18] also uses a complicated hierarchical feature aggregation technique and applies three different loss functions simultaneously. In ComposeAE[33], a novel embedding space that can seman-

tically tie representations from the text and image modalities was designed. The winning solutions [40, 29, 19] for the Fashion-IQ 2020 challenge employed more trivial tricks to achieve the best performance in this task by using careful hyperparameter tuning and model ensemble with Bayes optimization [31] to significantly improve the results. Although the aforementioned methods have focused on achieving the highest score on the benchmark, only a few studies have focused on the composition module itself [33, 2]. Because different aspects (e.g., *image/text encoder or loss function*) of *image and text composition* were addressed in recent related works [2, 29, 7, 6, 18], a naive comparison could lead to a misinterpretation. Therefore, our objective is not to pursue the best benchmark score. Instead, we are more interested in a “pure” comparison that focuses on the design of the composition module and a “fair” comparison that avoids the use of any trivial tricks to improve the score without explainable interpretation.

Graph Convolutional Network. The graph convolutional network (GCN) was first introduced in [22] to perform semi-supervised classification. The essential strength of the GCN is its ability to extract meaningful information encoded in the form of a structured graph from the relationships between the nodes. While most applications of GCN were limited to node classification in the early stage, many efforts [8, 24, 5, 23] have been made to use properly modified GCNs as joint training modules. In the most closely related work to ours, Chen *et al.* [8] applied GCN for multi-label classification by learning linear classifiers from the graph for projecting features into class labels. In that work, the word embeddings were used for the node feature matrix and the label co-occurrence was measured to determine the values for the graph edges. Although the effectiveness of GCN has been proved in many other studies [35, 34, 9], applying GCN for a new task such as *image-text composition* is not trivial. This is because the GCN requires a high quality graph. Building such meaningful graphs is tricky because a proper definition of the graph nodes and a careful strategy for encoding the relationships between the nodes are needed. In this paper, we introduce the application of a GCN for the *image-text composition* task for the first time. We define the nodes as *image-text* pairs and assign higher correlations to nodes that have target images with high visual similarity. Our approach is explained in detail in the following section.

3. Proposed Approach

In this section, we introduce our proposed method called the Residual Text and Image Composer (RTIC). The goal of the *image text composition* task is to combine the source image I^{src} and the text T by using a multi-modal composer $\psi(\cdot, \cdot)$ to generate a desired representation close to the representation of the target image I^{trg} . For this purpose, $\{I^{src}$,

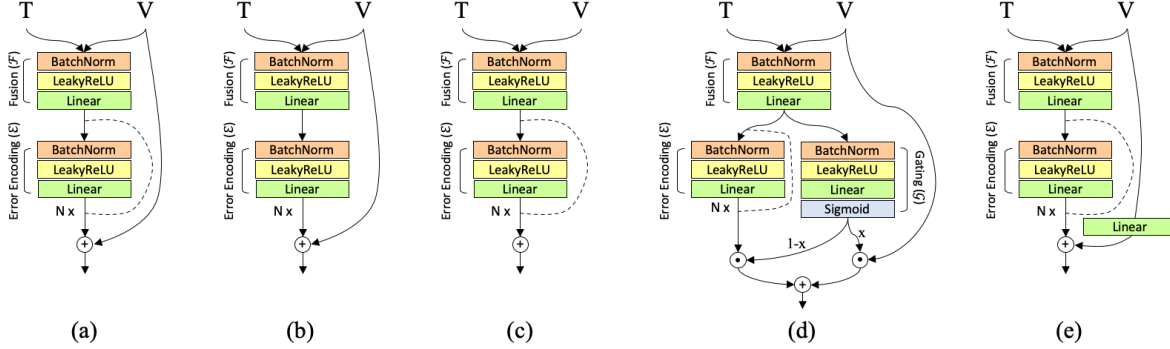


Figure 2. Alternative models are examined to justify our architecture design for the composition method. T and V indicate the representations extracted from the text and the image encoder, respectively. We conceptually illustrate the composition of layers for each blocks. The real composition is described in more detail in the Appendix.

T , and $I^{trg}\}$ triplets are required for supervision. Given a composition method such as RTIC, we denote the conventional training pipeline in which pairwise ranking loss (e.g., *triplet loss*) is applied on the ground-truth triplets as the main stream. The proposed GCN stream is an auxiliary module attached to the main stream. Our approach is based on two-stage training. In the first stage, the multi-modal composer, RTIC, is trained in the main stream. Then, in the second stage, a graph is built using the trained RTIC to configure the GCN stream and train the main stream model jointly with the GCN stream from scratch. Since the pre-trained composer in the first stage is only used for the graph construction as a preprocessing for GCN stream, the training in the second stage no longer requires the pre-trained composer once the graph is obtained. To be clearer, the composer in the main stream is trained in both stages, while the GCN stream is only attached to the main stream at the second stage for joint training.

3.1. Residual Text and Image Composer

RTIC is designed to learn the residual between the target and source image representations. The idea is that, given the images I^{src} and I^{trg} and the features v^{src} and v^{trg} of the source and the target, respectively, we consider the target v^{trg} as an addition of the source v^{src} and the residual h conditioned on the text feature t , which is represented as $h = \delta(v^{src}; t)$, where δ is a nonlinear mapping. Therefore, the final composed feature \tilde{v} is formulated as $\tilde{v} = v^{src} + h \simeq \psi(v^{src}; t) = v^{trg}$, assuming that $\psi(\cdot, \cdot)$ is an ideal composition module. In the RTIC, the residual h is considered as an error between the two different image features, v^{src} and v^{trg} , which is continuously distributed over the entire channel. The RTIC consists of three main components: a fusion block, an error encoding block, and a gating block. The fusion block \mathcal{F} combines two modalities, t and v^{src} , into a single representation $x = \mathcal{F}(v^{src}, t)$. Then, x is fed to the error encoding block \mathcal{E} and gating block \mathcal{G} to

obtain the final composed feature \tilde{v} as follows:

$$\begin{aligned} s &= \mathcal{G}(\mathcal{F}(v^{src}, t)) = \mathcal{G}(x), \\ \mathcal{X}^n &= \mathcal{X}^{n-1} + \mathcal{E}^n(\mathcal{X}^{n-1}), \quad \mathcal{X}^0 = x, \\ \tilde{v} &= (1 - s) \cdot \mathcal{X}^n + s \cdot v^{src} \simeq v^{trg}, \end{aligned} \quad (1)$$

where \mathcal{X}^n represents the output of the n -th error encoding block \mathcal{E}^n . Note that the output of the previous error encoding block \mathcal{X}^{n-1} is added to the next output using the skip connection. Figure 2 conceptually illustrates the flow to facilitate understanding. In all our experiments, n was set to four by default. For the next step, we follow the general pipeline of the other existing methods for the main stream, in which a pairwise ranking loss is applied using \tilde{v} as the anchor and v^{trg} as the positive. Following [33], we use the DML loss ($K=B$) for the pairwise ranking loss. Although we observed that a better overall score was achieved using the batch hard triplet loss [16], we intentionally used the DML loss because such a classification-based objective can effectively suppress undesirable effects caused by the sampling strategy. We refer interested readers to [33] for detailed definition of DML Loss. The structure finally chosen for the RTIC is architecture (d) in Figure 2. The details of our design choice are discussed in Section 4.2.

In summary, RTIC has two main differences from TIRG. First, RTIC uses channel-wise linear interpolation between the source image feature v^{src} and the residual h in which the sigmoid function is applied to the output of the gating block \mathcal{G} to determine the ratio. Second, RTIC employs a deeper architecture for error encoding by stacking n learning blocks in series using skip connections. RTIC is the second place solution to the Fashion-IQ 2020 challenge ¹. In the following section, we explain our proposed graph-based approach, RTIC-GCN, which is a further-improved method of RTIC.

¹<https://sites.google.com/view/cvcreative2020/fashion-iq>

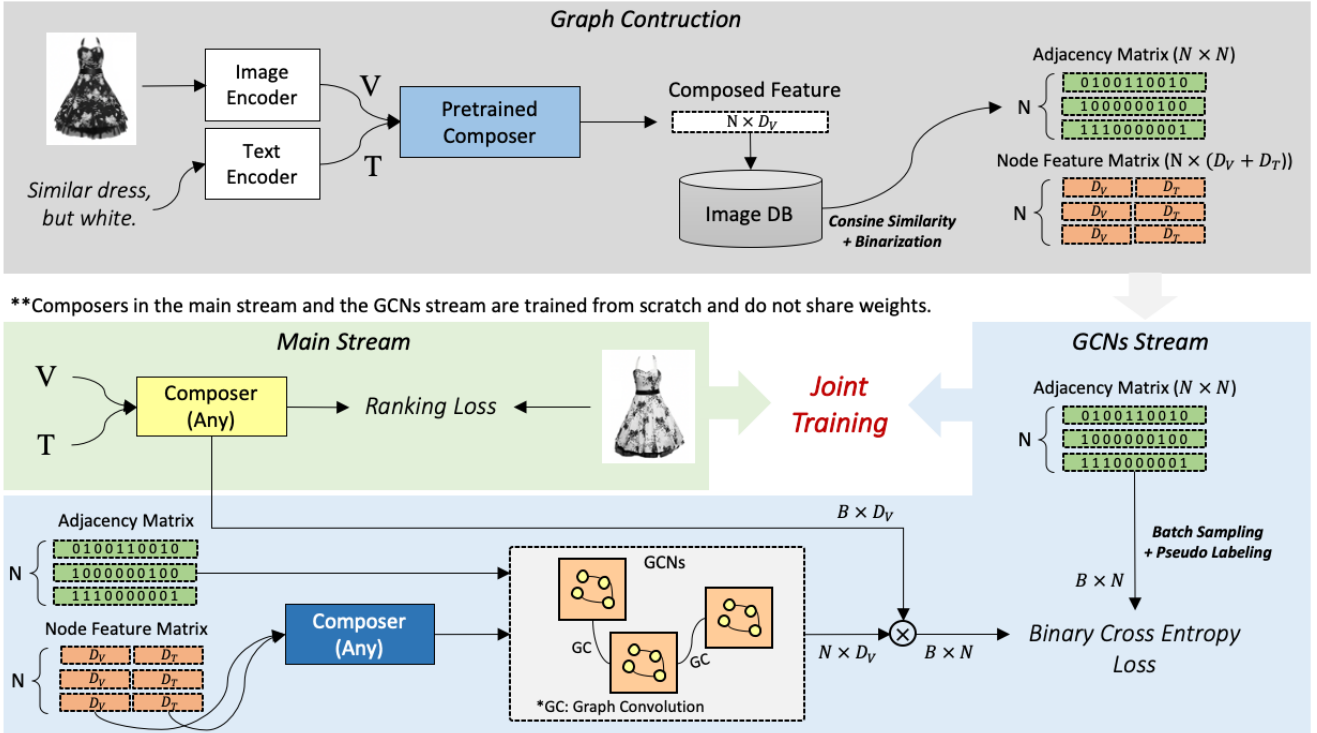


Figure 3. The pipeline for joint training with the GCN stream. The blue region indicates the GCN module, which can be attached to any existing composition method in a plug-and-play manner. Note that the weights between the two composers in each stream are not shared. We use \hat{A} for the GCN input and A' for the batch sampling and pseudo-labeling, following the notation in Section 3.2.

3.2. GCN as a Good Regularizer

One challenge in image-text composition is that an infinite number of perceptually acceptable image and text pairs exist, while the ground-truth triplets (I^{src} , I^{trg} , and T) in the training set reflect only a small fraction of these pairs. Such a scarcity of training pairs causes poor generalization. To resolve this, we introduce a novel method of using a graph convolutional neural network (GCN) as a regularizer by propagating information between adjacent neighbors. Our intuition is that, because there exists an unlimited number of ways to describe I^{trg} given I^{src} , we consider a group of $\{I^{src}, T\}$ pairs that describe a visually similar target image I^{trg} and are hence highly correlated with one another. For example, an image of a *red coat* with the text “it is blue” and an image of a *blue shirt* with the text “it is a coat” would both have an image of a *blue coat* as the target, which means that the two pairs are highly correlated. We model such relationships between pairs in the form of a graph by measuring the visual similarities between the target images of the triplets. Our intuition is conceptually illustrated in Figure 1.

Revisiting GCN. Before moving into the details, we briefly review how a GCN works. The core idea in a GCN is that the node representation is updated by propagating informa-

tion from the neighboring nodes based on graph-structured data. The goal of the GCN is to learn a nonlinear mapping $f(\cdot, \cdot)$ on the graph. The l -th layer of the GCN takes the node feature matrix $H^l \in R^{N \times D}$ and the correlation matrix $\Lambda \in R^{N \times N}$ as inputs, where N and D indicate the number of nodes and the dimensionality of the node features, respectively. The operation on each layer of the GCN can be represented as

$$\begin{aligned} \hat{\Lambda} &= D^{\frac{1}{2}} \Lambda D^{-\frac{1}{2}}, \\ H^{l+1} &= h(\hat{\Lambda} H^l W^l), \end{aligned} \quad (2)$$

where D represents a diagonal matrix of Λ and W^l indicates the transformation matrix of the l -th layer to be learned. We used ReLU for the activation function h . For more details, we refer interested readers to [22].

Graph construction. Most importantly, we define each graph node as an *image-text* pair, which means that the N ground-truth pairs in the training data creates N graph nodes in total. Assuming that we have a learned image encoder $\phi_{pretrained}$ trained in the first stage, we model the correlations between the nodes (*image-text* pairs) by measuring the cosine similarities between the target features of the corresponding nodes $\mathcal{V} = \{v_1^{trg}, \dots, v_N^{trg}\}$, where the target features of the i -th node are obtained by

$v_i^{trg} = \phi_{pretrained}(I_i^{trg})$. As a result, we obtain a symmetrical correlation matrix $\Lambda \in R^{N \times N}$ because the cosine similarity measure has a commutative property and the similarity with the self-node is always 1. Then, we binarize Λ with the threshold τ to filter out the noisy edges:

$$\Lambda'_{ij} = \begin{cases} 1, & \text{if } \Lambda_{i,j} \geq \tau \\ 0, & \text{if } \Lambda_{i,j} < \tau, \end{cases} \quad (3)$$

where τ is a hyperparameter set to the value that makes the average number of activated edges in each node 12% of N . Chen *et al.* [8] addressed the over-smoothing problem that occurs when each node feature is repeatedly updated using its own features and those of the neighboring nodes by employing a re-weighting strategy. We follow the same scheme with a slight modification:

$$\Lambda''_{ij} = \begin{cases} 1, & \text{if } i = j \\ 0.25 / \sum_{j=1, i \neq j}^C \Lambda'_{ij}, & \text{if } i \neq j. \end{cases} \quad (4)$$

Finally, Λ'' is re-normalized: $\hat{\Lambda} = D^{\frac{1}{2}} \Lambda'' D^{-\frac{1}{2}}$, as described in Equation 2. The full graph construction algorithm is given in Algorithm 1.

Algorithm 1 Graph construction algorithm for encoding the contextual similarity between the nodes represented by the *image-text* pairs

```

1: Input: Image encoder  $\phi$ , text encoder  $\lambda$ , composer  $\psi$ ,  $N$  triplets of image and text  $X = \{(I_i^{src}, T_i, I_i^{trg}) : i \in (1, \dots, N)\}$ .
2:  $(\mathcal{H}, \Omega) \leftarrow ([], [])$ 
3: for  $i = 1$  to  $N$  do
4:   // extract image and text representations
5:    $v_i^{src} \leftarrow \phi(I_i^{src})$ ,  $t_i \leftarrow \lambda(T_i)$ ,  $v_i^{trg} \leftarrow \phi(I_i^{trg})$ 
6:    $\mathcal{H}.append(v_i^{src} \oplus t_i)$  // node feature matrix
7:    $\Omega.append(v^{trg})$  // create feature DB
8: end for
9:  $\Lambda \leftarrow cosine\_similarity(\Omega \cdot \Omega^T)$  // correlation matrix
10:  $\Lambda' \leftarrow binarized(\Lambda)$  // thresholding
11:  $\Lambda'' \leftarrow reweighted(\Lambda')$  // to avoid over-smoothing
12:  $\hat{\Lambda} \leftarrow normalized(\Lambda'')$  // to keep the scale
13: Output: Normalized correlation matrix  $\hat{\Lambda} \in R^{N \times N}$ , node feature matrix  $\mathcal{H} \in R^{N \times (D_V + D_T)}$ .
```

Joint training with GCN stream. Denoting the general training pipeline (*e.g.*, *training RTIC with ranking loss*) as the main stream, the GCN stream can be defined as an auxiliary module that aims to improve the mainstream model by injecting additional signals in a semi-supervised manner. Once the graph is constructed, the GCN stream can be configured and jointly trained with the main stream. The composers in each stream in Figure 3 are randomly initialized and the graph is the only source of information that the

model can benefit from during training. The GCN stream is configured using the output correlation matrix $\hat{\Lambda} \in R^{N \times N}$ and the node feature matrix $\mathcal{H} \in R^{N \times (D_V + D_T)}$, where N is the number of $\{I^{src}, T\}$ pairs, and D_V and D_T are the output feature dimensions of the image and the text encoders, respectively. For the next step, the image and text feature matrices $\bar{v} \in R^{N \times D_V}$, $\bar{t} \in R^{N \times D_T}$ are split from \mathcal{H} and fed to a randomly initialized new composer in the GCN stream that converts \mathcal{H} into a matrix of composed features $\tilde{\mathcal{H}} \in R^{N \times D_V}$. Note that the weights of the composers in each stream are not shared because the two composers will have different input distributions as the training proceeds. Finally, $\tilde{\mathcal{H}}$ and $\hat{\Lambda}$ are forwarded by the GCN layers to obtain the GCN stream output $\mathcal{W} \in R^{N \times D_V}$.

We inject information from the GCN stream into the main stream in the form of node classifications [8]. Given a mini-batch B , we perform matrix multiplication between the output of the main stream $\mathcal{X} = \{\tilde{v}_1, \dots, \tilde{v}_B\} \in R^{B \times D_V}$ and the output of the GCN stream $\mathcal{W} \in R^{N \times D_V}$ to obtain the logits $x = \mathcal{X} \times \mathcal{W}^T \in R^{B \times N}$. Then, we use the binary cross-entropy loss to perform a node classification on the N graph nodes. This process can be considered as finding the most relevant neighbors for a batch of queries among all the $\{I^{src}, T\}$ pairs that exist in the graph. For supervision, we sample B as the number of one-hot vectors $c \in R^{B \times N}$ on the fly from Λ' according to the unique key assigned to the pairs in the mini-batch. The terminologies, batch sampling, and pseudo labeling in this process are indicated in Figure 3. Finally, the loss for the joint training is obtained as the sum of the pairwise ranking loss in the main stream and the binary classification loss in the GCN stream, $\mathcal{L}_{final} = \lambda_{pair} \cdot \mathcal{L}_{pair} + \lambda_{bce} \cdot \mathcal{L}_{bce}$, where $(\lambda_{pair}, \lambda_{bce}) = (1.0, 1.0)$ is used by default. Although the GCN stream requires additional GPU memory, as shown in Figure 5, the GCN stream is used only for the training and is simply removed for the inference. This means that no additional model parameters are required for the inference model.

4. Experiment

4.1. Experimental Settings

In this section, we explain our experimental settings in detail. We emphasize the choice of datasets used for training and evaluation, the extraction of the image and text representations, and the control of the training environment.

4.1.1 Datasets

Fashion-IQ. [14] is a fashion product retrieval dataset that consists of images crawled from *amazon.com* and natural language-based descriptions of one or more visual characteristics relating the source and target images. It contains three categories, namely, dresses, topees, and shirts. Fol-

Table 1. Benchmark score on the Fashion-IQ dataset evaluated with the suggested training standard. The † marks indicates the methods that were trained and evaluated with the best settings in their respective papers.

Method	Average (R@10 + R@50) / 2	Shirt		Dress		Toptee	
		R@10	R@50	R@10	R@50	R@10	R@50
Param Hashing [26]	26.54 \pm 0.20	12.26 \pm 0.58	32.83 \pm 0.66	15.48 \pm 0.53	39.13 \pm 0.52	17.66 \pm 0.39	41.89 \pm 0.68
MRN [20]	28.83 \pm 0.18	14.50 \pm 0.43	35.43 \pm 0.39	16.60 \pm 0.47	40.50 \pm 0.76	20.22 \pm 0.55	45.74 \pm 0.26
FiLM [28]	28.72 \pm 0.32	13.56 \pm 0.33	35.64 \pm 0.94	16.78 \pm 1.04	40.77 \pm 0.98	19.91 \pm 0.62	45.64 \pm 0.60
TIRG [33]	30.71 \pm 0.25	16.12 \pm 0.39	37.69 \pm 0.70	19.15 \pm 0.61	43.01 \pm 0.91	21.21 \pm 0.70	47.08 \pm 0.49
ComposeAE [2]	19.61 \pm 0.41	9.96 \pm 0.60	25.14 \pm 0.88	10.77 \pm 0.70	28.29 \pm 0.49	12.74 \pm 0.67	30.79 \pm 0.62
VAL [7]	27.16 \pm 0.24	13.62 \pm 0.59	33.81 \pm 0.95	16.03 \pm 0.58	39.07 \pm 0.64	18.02 \pm 0.52	42.40 \pm 0.44
Block [4]	27.84 \pm 0.34	13.67 \pm 0.69	35.35 \pm 0.77	16.01 \pm 0.54	39.61 \pm 0.56	18.39 \pm 0.74	44.03 \pm 0.58
Mutan [3]	29.34 \pm 0.22	15.20 \pm 0.82	36.17 \pm 0.42	17.46 \pm 0.56	42.14 \pm 0.46	20.04 \pm 0.62	45.03 \pm 0.62
MLB [21]	27.12 \pm 0.49	13.30 \pm 0.44	33.16 \pm 0.43	15.33 \pm 0.50	39.71 \pm 0.82	17.75 \pm 0.40	43.51 \pm 1.10
MFB [37]	27.98 \pm 0.21	13.94 \pm 0.67	34.37 \pm 0.38	16.60 \pm 0.58	40.36 \pm 0.90	18.36 \pm 0.56	44.24 \pm 0.65
MFH [38]	27.96 \pm 0.27	13.87 \pm 0.59	35.04 \pm 0.22	15.95 \pm 0.61	40.16 \pm 0.84	18.52 \pm 0.63	44.21 \pm 0.75
MCB [11]	29.28 \pm 0.29	14.77 \pm 0.75	36.34 \pm 0.48	17.43 \pm 0.57	41.69 \pm 0.63	19.96 \pm 0.75	45.46 \pm 1.01
RTIC	31.28 \pm 0.22	16.93 \pm 0.45	38.36 \pm 0.61	19.40 \pm 0.50	43.51 \pm 0.90	21.58 \pm 0.70	47.88 \pm 0.90
RTIC-GCN	31.68 \pm 0.30	16.95 \pm 0.59	38.67 \pm 0.74	19.79 \pm 0.41	43.55 \pm 0.24	21.97 \pm 0.71	49.11 \pm 0.87
JVSM [†] [6]	19.26	12.00	27.10	10.70	25.90	13.00	26.90
TRACE w/ BERT [†] [18]	34.38	20.80	40.80	22.70	44.91	24.22	49.80
VAL w/ GloVe [†] [7]	35.38	22.38	44.15	22.53	44.00	27.53	51.68
CurlingNet [†] [36]	38.45	21.45	44.56	26.15	53.24	30.12	55.23
RTIC [†]	38.09	22.03	45.29	27.37	52.95	27.33	53.60
RTIC-GCN [†]	39.00	22.72	44.16	27.71	53.50	29.63	56.30

lowing the same protocol as [14], we used 46,609 images and 18,000 triplets for training, and 5,373 images and 6,016 triplets for evaluation.

Shoes. [13] is a dialog-based interactive retrieval dataset in which the images were originally crawled from *like.com* and additionally tagged with natural language-based relative captions. Following [13], we used 10,000 images and 8,990 triplets for training, and 4,658 images and 1,761 triplets for evaluation.

Birds-to-Words. [10] consists of 3,520 bird images from *iNaturalist* along with human-annotated natural language captions that describe the differences between pairs of images. Each text description is longer (average of 31 words) than those of the previous two datasets and has a richer description. We used 2,835 images and 12,805 triplets for training, and 361 images and 1,556 triplets for evaluation.

4.1.2 Image and text representation

Although the main focus of our work is on the composition of the two modalities, we observe that even a small modification of the text and the image encoders greatly affects the final performance. Therefore, we briefly describe our settings for learning the text and image representations.

Text Representation. We learned the sentence embedding from scratch using LSTM [17]. To be specific, we tokenized the captions using a simple whitespace tokenizer and then built a word-to-vector vocabulary. Although applying GloVe [27] initialization on the word vectors can improve the result, we intentionally omitted the use of this technique

and retained our training setting as the baseline. The word embeddings were forwarded by the 1-layered LSTM, and the outputs were max-pooled to obtain the sentence embedding. Finally, the outputs were projected onto the desired dimensions using a fully connected layer.

Image Representation. ResNet-50 [15] was used as the backbone for the image encoder. Global average pooling (GAP) was applied to the output of the last convolutional layer, followed by a fully connected layer. We did not use a shallower backbone such as ResNet-18 because this made the performance difference between the composition methods relatively trivial owing to the limited ability of the backbone to learn representations.

4.1.3 Training standard

All our experiments were performed in a restricted environment to maximally suppress the misleading performance gain from parameter optimization. While such a strict setting degrades the overall benchmark scores on the dataset, it can make the results more reliable and objective for comparison. For example, we used the DML Loss [33] for the ranking loss because it is unaffected by the choice of sampling strategy. No initialization such as GloVe or BERT was used for the word embeddings because the effect of the initialization is highly coupled with the type of tokenizer used and the quality of the pretrained word embeddings. We also used SGD with a fixed $lr=0.01$ for the optimizer with no parameter tuning, because adjusting lr can increase the overall score significantly, as described in Table 5. Lastly, we re-

port the average score of eight trials for all our experiments to obtain more precise and clearer trends. The other aspects of the experiments are described in more detail in the Appendix.

4.2. Performance Evaluation

Performance comparison. For evaluation, we measured the top-k recall (R@K) on different benchmarks while keeping strictly to our established standard during training. While following our settings led to relatively low scores, the composition methods can be compared fairly in this constrained environment. Table 1 and Table 2 show the results for the three benchmarks. We intentionally omitted some recent methods [6, 18, 7, 36] because these works do not solely focus on the composition method itself but also on other aspects such as the image/text encoders and loss functions. Instead, we compared our method with other methods trained with our own best settings. Although this approach might not be sufficiently objective, it would still provide some naive insights.

Table 1 shows that RTIC already achieves the highest score among the various methods, and that joint training with the GCN stream (RTIC-GCN) further improves the score by approximately 0.4% Δ . The scores for the methods marked by \dagger were obtained using the best settings for the methods reported in their respective papers. To achieve the state-of-the-art score, we gradually adjusted the detailed training parameters, as described in Table 5. We did not employ trivial tricks that might improve the score, such as aggregating multiple local features or concatenating the intermediate features, because such tricks excessively increase the memory usage and model complexity. Finally, we achieved a 0.55% Δ improvement compared to the previous state-of-the-art.

Table 2. Benchmark scores on Shoes and Birds-to-Words dataset.

Method	Shoes		Birds-to-Words	
	R@10	R@50	R@10	R@50
Param Hashing [26]	36.37 \pm 0.47	67.24 \pm 0.88	27.54 \pm 1.57	58.43 \pm 1.59
MRN [20]	37.51 \pm 0.47	68.66 \pm 0.75	37.33 \pm 1.38	68.97 \pm 1.35
Film [28]	36.74 \pm 0.56	68.47 \pm 0.43	32.58 \pm 1.59	65.80 \pm 1.48
TIRG [33]	40.40 \pm 0.69	70.65 \pm 0.65	33.83 \pm 1.53	65.96 \pm 1.56
ComposeAE [2]	31.25 \pm 0.67	60.30 \pm 0.33	29.60 \pm 0.99	59.82 \pm 1.83
VAL [7]	36.91 \pm 0.75	67.16 \pm 0.73	28.65 \pm 1.48	60.22 \pm 1.31
Block [4]	36.82 \pm 0.61	67.79 \pm 0.51	26.19 \pm 1.63	57.89 \pm 1.37
Mutan [3]	39.13 \pm 0.73	69.86 \pm 0.53	32.15 \pm 1.83	62.36 \pm 1.59
MLB [21]	35.35 \pm 0.88	67.30 \pm 0.57	30.93 \pm 1.77	63.22 \pm 1.72
MFB [37]	36.59 \pm 1.54	67.58 \pm 0.49	30.43 \pm 1.92	64.03 \pm 1.69
MFH [38]	35.85 \pm 1.20	68.07 \pm 1.07	31.11 \pm 2.18	64.18 \pm 1.93
MCB [11]	38.70 \pm 0.66	68.96 \pm 0.69	30.86 \pm 1.44	62.80 \pm 2.12
RTIC	43.66 \pm 0.67	72.11 \pm 0.51	37.40 \pm 1.36	66.97 \pm 1.70
RTIC-GCN	43.38 \pm 0.88	72.09 \pm 0.48	37.56 \pm 1.12	67.72 \pm 1.46

Architecture verification. In Table 3, we verify our architecture design by comparing the possible variants of the RTIC structure and analyzing the effect of each component. The best structure is (d), which consistently shows the best score, followed by (a) with a marginal gap. The main fea-

ture of architecture (d) is the use of a channel-wise gating mechanism that performs linear interpolation between the image feature and the residual. Interestingly, the performance drops significantly without the skip connections inside the error encoding stack ((a) vs. (c)). The score degradation caused by removing the skip connections from the visual representation is relatively small ((a) vs. (b)). Adjusting the latent space of the image by attaching an additional projection layer is not helpful ((a) vs. (e)). Finally, (d) was chosen for the final architecture design of the RTIC.

Table 3. Comparison between alternative models (a-e) on *image-text composition* task. The compared structures are illustrated in Figure 2.

	(R@10 + R@50) / 2		
	Fashion IQ	Shoes	Birds-to-Words
(a)	31.28 \pm 0.22	57.58 \pm 0.40	51.73 \pm 0.49
(b)	24.71 \pm 0.69	53.07 \pm 0.51	46.21 \pm 1.84
(c)	30.44 \pm 0.23	55.43 \pm 0.60	48.38 \pm 0.40
(d)	31.41 \pm 0.41	57.73 \pm 0.45	52.24 \pm 1.06
(e)	30.02 \pm 0.25	55.81 \pm 0.54	48.42 \pm 1.55

Effect of graph quality. We examine the effect of the graph quality on the joint training with the GCN stream in Table 4. Assuming that the pretrained RTIC can construct more precise graphs than the other methods based on the results in Table 1, we compare the improvements of four existing methods trained with the GCN stream (*TIRG-GCN*, *MRN-GCN*, *ComposeAE-GCN*, *Param Hashing-GCN*) using the graphs constructed by the methods themselves and those constructed by the RTIC. All the methods benefitted from training with the GCN stream, which implies that the GCN stream is a sufficiently general method that can be attached to any composition module. Moreover, the result shows that a higher graph quality consistently results in a larger gain, which implies that the single-model score can be improved with higher quality graphs.

Table 4. The performance boost evaluated on Fashion-IQ when trained w/ or w/o the GCN stream. w/ GCN, Self and w/ GCN, RTIC indicate that the graph of the GCN stream is constructed using the compared method itself and using the RTIC, respectively.

Method	-	w/ GCN, Self	w/ GCN, RTIC	max. Δ
TIRG	30.71	31.26	31.39	+2.21%
MRN	28.83	28.92	29.28	+1.56%
ComposeAE	19.61	29.70	29.43	+33.97%
Param Hashing	26.54	26.86	26.89	+1.31%

Ablation study. In this section, we describe the optimization process of our best setting used for the retrieval challenge and discuss how the final score can be affected by modifying the training parameters trivially. The results are presented in Table 5. Starting from the baseline score of 33.24, the single-model performance could be improved by up to 13% simply by optimizing the training parame-

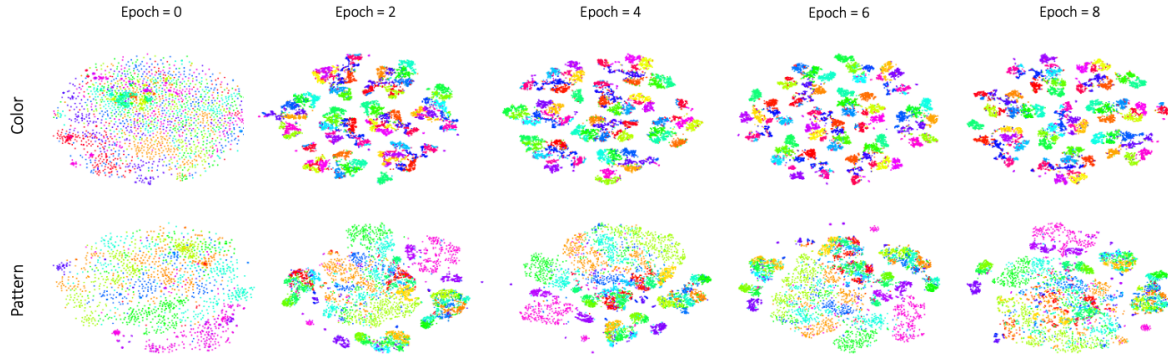


Figure 4. t-SNE visualization of the error encoding block output.

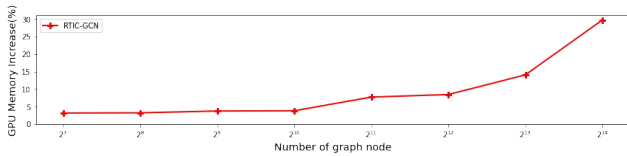


Figure 5. Additional GPU memory required for GCN stream in percents.

ters. Following our optimization, we obtained a score of 37.18 for TIRG, which outperforms the more recent methods. This strongly implies that a fixed baseline standard for training is required to fairly compare the methods across papers.

Table 5. The variation of the single-model performance with different training settings. The optimizer (from SGD to AdamW), the text encoder (from LSTM to 2-layered LSTM+GRU), and the embedding feature dimension of the composed feature (from 512 to 2048) are changed gradually to maximize the final score.

Training details	Validation
Baseline (RTIC)	33.24
+ Replace optimizer	34.89 (+4.96%)
+ Increase embedding dimension	36.79 (+5.45%)
+ Replace text encoder	37.72 (+2.47%)
+ Spell correction	38.22 (+1.33%)

Trade off. Although training with the GCN stream is a well-generalized technique that can consistently improve the score of any existing method as shown in Table 4, back-propagating gradients through the GCN layers requires additional GPU memory for training. Figure 5 shows the additional GPU memory required for joint training with the GCN stream. We gradually increased the number of graph nodes and measured the relative increase in GPU memory used when the GCN stream was attached to the main stream. We report the relative rather than the absolute increases because the latter vary with the batch size and network complexity. In the inference phase, we no longer re-

quire the GCN layers for inference, which means that the GCN stream does not slow down the inference speed at all.

4.3. Visualization

Figure 4 illustrates the t-SNE [32] visualization of the error-encoding block outputs from the RTIC. We sample 250 images from each of the eight different color classes (*yellow, black, red, blue, green, brown, orange, pink*) and condition the images with the different class labels (*e.g. blue image with text “yellow”*) instead of the captions for the query. We then extract the output of the error-encoding block and visualize the distribution. It should be noted that images in the same class could have different attributes. For example, the images in the “blue” class will have the same color but different patterns (*e.g., striped, dotted, or floral*). Nevertheless, Figure 4 shows that the clusters are clearly formed, which indicates that the error encoding block successfully disentangles the other attributes from the representation when it is conditioned on the specific color-related text in the query. We also performed the same experiments with eight different pattern classes and observed consistent results.

5. Conclusion

In this paper, we proposed a novel architecture, RTIC, specifically designed for the *image-text composition* task. Moreover, we introduced the GCN stream graph-based regularization technique, which can be attached to any kind of composer in a plug-and-play manner. The GCN stream is a well-generalized technique that consistently improves the results of existing composition methods. Finally, we achieved a state-of-the-art score on the *image-text composition* task without using additional tricks, such as hierarchical feature aggregation or multiple loss functions. To avoid unexpected effects, we intentionally restricted our training environment. Therefore, all our experiments were performed based on the established training standard for a fair comparison.

A. Notation

Symbol/Notation	Definition
I^{src}	Source image
I^{trg}	Target image
T	Text description
$\psi(\cdot, \cdot)$	Text-Image multi-modal composer
v^{src}	Visual feature extracted from source image
v^{trg}	Visual feature extracted from target image
$\delta(\cdot, \cdot), f(\cdot, \cdot)$	Non-linear mapper
\tilde{v}	Final composed feature
\mathcal{F}	Fusion block
\mathcal{E}	Error encoding block
\mathcal{G}	Gating block
n	Number of error encoding blocks in stack
\mathcal{X}^n	Output of the n -th error encoding block in stack
K	Number of negative samples in mini-batch
B	Batch size
H	Node feature matrix
Λ	Correlation matrix
N	Number of nodes
D_V	Dimensionality of visual features
D_T	Dimensionality of text features
W	Transformation matrix
\mathcal{V}	Set of target image features
λ	Text encoder
ϕ	Image encoder
Λ'	Binarized correlation matrix
τ	Threshold for correlation matrix binarization
Λ''	Re-weighted correlation matrix
$\hat{\Lambda}$	Re-normalized correlation matrix
Ω	Collection of image features
\mathcal{X}	Output of main stream
\mathcal{W}	Output of GCN stream
c	One hot vector

B. Architecture

Table 6. Detailed configuration for RTIC architecture.

		input dim	output dim
Fusion block (\mathcal{F})	Concat (dim=1)	D_T, D_V	$D_T + D_V$
	BatchNorm1d	$D_T + D_V$	$D_T + D_V$
	LeakyReLU	$D_T + D_V$	$D_T + D_V$
	Linear	$D_T + D_V$	D_V
Error encoding block (\mathcal{E})	Linear	D_V	$D_V/2$
	BatchNorm1d	$D_V/2$	$D_V/2$
	LeakyReLU	$D_V/2$	$D_V/2$
	Linear	$D_V/2$	$D_V/2$
	BatchNorm1d	$D_V/2$	$D_V/2$
	LeakyReLU	$D_V/2$	$D_V/2$
	Linear	$D_V/2$	D_V
Gating block (\mathcal{G})	Linear	D_V	D_V
	BatchNorm1d	D_V	D_V
	LeakyReLU	D_V	D_V
	Linear	D_V	D_V
	Sigmoid	D_V	D_V

C. Learning Curves

We compare the learning curves of RTIC when it is trained w/ or w/o the GCN stream. The result is shown in Figure 6. The graph shows that the use of the GCN stream

can achieve a clear performance improvement against the other. Such tendency is consistent in that similar results are also observed using the other composition methods (e.g., TIRG).

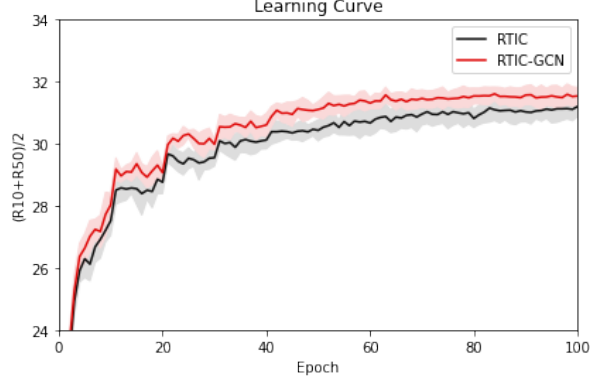


Figure 6. Learning curves of RTIC and RTIC-GCN.

D. Study on Other Possible Variants

Our proposed GCN stream is a semi-supervised technique based on the structured graph. Since there exist various ways to utilize pseudo labels for training, we explore if other semi-supervised learning techniques can be employed for this task. We examine two different baselines to compare with GCN stream: *Linear+BCE* and *Pseudo Pairs*.

Linear+BCE. Since the goal of the GCN stream is to learn a projection matrix $\mathcal{W} \in R^{D_V \times N}$, it is equivalent to learning a single-layer perceptron with no bias. Therefore, one can attach a linear layer instead of GCN layers behind the main stream and use binary cross-entropy (BCE) loss with pseudo labels sampled from A' as same as GCN stream.

Pseudo Pairs. Using the graph, we can also generate pseudo pairs $\{I^{src}, T, I^{trg}\}$ pairs. The idea is that if two pairs have visually similar target image which has high cosine similarity above a certain threshold, we switch the I^{trg} in two pairs. In this way, we double the number of $\{I^{src}, T, I^{trg}\}$ pairs in the train split of Fashion-IQ, and train RTIC in the main stream without GCN stream.

The result is shown in Table 7. The result shows that both *Linear+BCE* and *Pseudo Pairs* do not help training compared to the baseline that does not use any semi-supervised techniques. Only the GCN stream improves the result by 0.4%p. It implies that simply applying BCE loss as auxiliary supervision does not improve the score (*Linear+BCE*). Moreover, automatically generated pseudo pairs should be carefully considered because the noise degrades the score significantly (*Pseudo Pairs*). This experiment shows that the performance gain due to the GCN stream is originated from not only the use of binary classification loss for auxiliary supervision but also a carefully designed GCN module

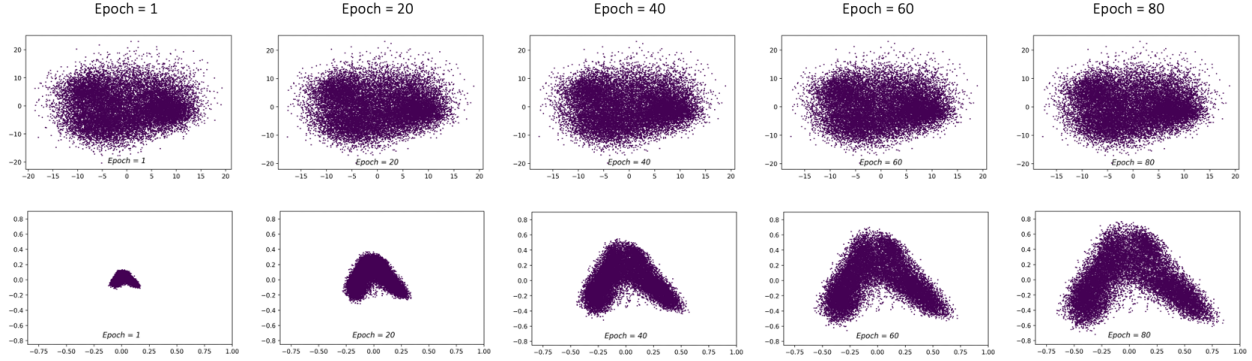


Figure 7. PCA visualization of the feature distribution in the GCN stream for each epoch. The first and second rows represent the feature distribution in the GCN stream before and after it is forwarded by GCN layers respectively.

indeed.

Table 7. Comparison with other semi-supervised learning techniques. We measure $(R@10 + R@50) / 2$ for the score.

Method	Score
Baseline	31.28 ± 0.22
Linear+BCE	27.44 ± 0.40
Pseudo Pairs	23.73 ± 0.18
GCN stream	31.68 ± 0.30

E. Analysis on Feature Distribution

No weight sharing between composers. The two composers in main stream and GCN stream do not share the weights during the training. This is because the input for the GCN stream, \mathcal{H} , is static values while the input for the main stream which is the representations learned by the image and text encoders is updated dynamically as the training proceeds. Such discrepancy between the input distributions of two composers degrades the performance if the weights are shared. Although we train two composers independently, the GPU memory required for training trivially increases because the composer has a small number of parameters.

Distribution before and after GCN layers. Figure 7 shows the PCA analysis on the feature distribution in the GCN stream before and after it is forwarded by GCN layers. The GCN layer converts the original feature distribution (*first row*) extracted by the image and text encoders trained in the first stage into the more structured form of distribution (*second row*), which implies the features are projected to be more distinguishable from each other. As the training proceeds, the features after the GCN layers are spread into space in a wider range.

F. Naive comparison with feature fusion methods.

We apply RTIC to the *feature fusion* task in this section. The Table 8 shows the result on widely used benchmarks, VQA 2.0 [12] and VRD [25]. We followed the training and testing environment with default parameters provided by the publicly released code ². The result shows that the methods designed for the *image text composition* task (*TIRG* and *RTIC*) are less effective for the *feature fusion* task (*BLOCK* vs. *RTIC*). Our interpretation is that since the *image text composition* methods are forced to embed the composed feature into the image feature space, it is considered as a redundant constraint in the *feature fusion* task which degrades the performance.

G. Score Inconsistency across Papers

Table 10 shows the inconsistency in reported scores across papers. We mainly investigate the score of TIRG [33] because it is the most widely used method for comparison in various studies. We found a significant gap between the reported scores which is the reason we address the need for a standard for training to ensure objectiveness and fairness in performing comparisons across papers.

Table 10. TIRG scores reported across papers.

$(R@10+R@50)/2$	Fashion-IQ	Fashion200K	Shoes
[7]	27.39	53.90	57.42
[2]	20.15	53.15	-
[18]	19.95	-	38.79
[6]	15.27	51.95	-
<i>max. Δ</i>	12.13	1.95	18.63

²<https://github.com/Cadene/block.bootstrap.pytorch>

Table 8. PP: Phrase Prediction, PD: Phrase Detection, RD: Relationship Detection task. The comparison with the feature fusion methods on two benchmarks (VQA 2.0 [12] and VRD [25]). We measure the accuracy for VQA 2.0 and R@50 for VRD.

	VRD			VQA 2.0 (<i>test-std</i>)			
	Phrase prediction	Phrase detection	Relationship detection	All	Yes/no	Num	Other
BLOCK	86.46	22.96	19.26	66.77	83.74	46.70	56.83
Mutan	85.00	12.10	7.96	-	-	-	-
MLB	84.85	19.08	15.55	40.59	61.19	38.48	23.14
MFB	82.46	23.99	16.84	38.50	61.18	32.35	20.16
MFH	83.42	24.01	16.89	-	-	-	-
MCB	84.24	18.54	12.65	41.65	73.83	34.66	15.24
TIRG	70.42	13.50	9.43	54.03	73.75	34.24	41.39
RTIC	80.17	16.48	11.21	47.00	61.17	26.01	39.49

Table 9. The baseline standard for training and testing.

	Training Standard
Image Encoder	ResNet50 (pretrained on ImageNet, output shape: 32 x 1024, avg-pooled)
Text Encoder	LSTM (num_layers: 1, input_size: 1024, hidden_size: 1024, output shape: 32 x 1024, max-pooled)
Image Size / Crop Size	256 / 224
Image Transform (Train)	ResizeWithPadding, RandomCrop, RandomHorizontalFlip, RandomAffine, Normalize
Image Transform (Test)	ResizeWithPadding, CenterCrop, Normalize
Optimizer	SGD
Loss	DML loss, K = B [33]
Training Epochs	100
Learning rate	0.01
Learning rate decay	policy: StepLR, factor: $1/\sqrt{2}$, step_size: 10
Others	No spell correction, No initialization with GloVe
Metric	Average Recall@K over 8 trials

H. Suggested Training Standard

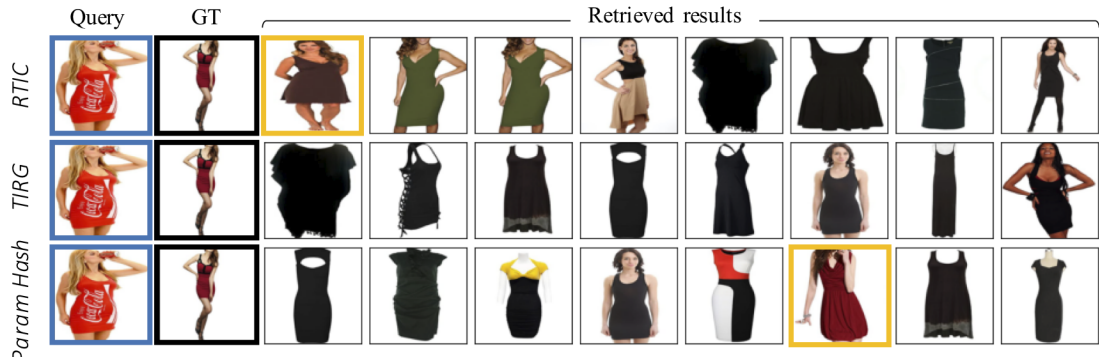
In Table 9, we suggest a baseline for training to accomplish a fair comparison. We keep the image and text encoder as simple as possible while keeping the complexity of encoders high enough to represent the visual and contextual information. The image is resized to 256×256 with padding while keeping the ratio, then cropped to 224×224 . We use DML loss (K=B) suggested in [33], mainly because it can suppress undesirable effects caused by the sampling strategy. According to the technical reports of the retrieval challenge, spell correction increases the result significantly. Moreover, initializing word embeddings with GloVe or BERT provides better generalization when the embeddings are fine-tuned. However, we omit such auxiliary techniques to keep our standard simple. We strongly suggest using the metrics that are averaged over eight trials, because the scores severely fluctuate even between models trained with the same training parameters.

I. Qualitative Result

The image retrieval result of the top 8 candidates is illustrated in Figure 8. The examples show that even though a ground-truth I^{src}, T, I^{trg} pair is defined, the text can

not fully describe the entire aspects of the target image. Therefore, the answer can be multiple similarly-looking items that are perceptually acceptable. Ideally, the model is guided to obtain clues for the other attributes that are not described by the text based on the source image.

Q: is a darker shade, It is darker and more plain



Q: is longer, is long and has a blue and white pattern



Q: is mustard colour and longer, is yellow and longer



Q: is visually aesthetic, has a flowered pattern

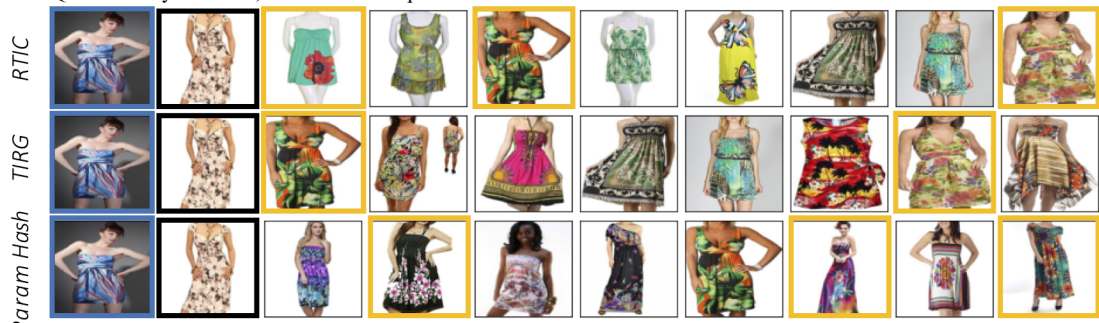


Figure 8. Top-8 retrieval examples of RITC, TIRG, and Parameter Hashing. The blue and the black border indicate the query and the ground-truth respectively. The red border means the answer is correctly found. The orange border is means the image is not the answer but perceptually acceptable.

References

[1] Kenan E Ak, Ashraf A Kassim, Joo Hwee Lim, and Jo Yew Tham. Learning attribute representations with localization for flexible fashion search. In *Proceedings of the IEEE conference on computer vision and pattern recognition*, pages 7708–7717, 2018. 1

[2] Muhammad Umer Anwaar, Egor Labintcev, and Martin Kleinsteuber. Compositional learning of image-text query for image retrieval. In *Proceedings of the IEEE/CVF Winter Conference on Applications of Computer Vision*, pages 1140–1149, 2020. 1, 2, 6, 7, 10

[3] Hedi Ben-Younes, Rémi Cadene, Matthieu Cord, and Nicolas Thome. Mutan: Multimodal tucker fusion for visual question answering. In *Proceedings of the IEEE international conference on computer vision*, pages 2612–2620, 2017. 1, 2, 6, 7

[4] Hedi Ben-Younes, Rémi Cadene, Nicolas Thome, and Matthieu Cord. Block: Bilinear superdiagonal fusion for visual question answering and visual relationship detection. In *Proceedings of the AAAI Conference on Artificial Intelligence*, volume 33, pages 8102–8109, 2019. 1, 2, 6, 7

[5] Jintai Chen, Biwen Lei, Qingyu Song, Haochao Ying, Danny Z Chen, and Jian Wu. A hierarchical graph network for 3d object detection on point clouds. In *Proceedings of the IEEE/CVF Conference on Computer Vision and Pattern Recognition*, pages 392–401, 2020. 2

[6] Yanbei Chen and Loris Bazzani. Learning joint visual semantic matching embeddings for language-guided retrieval. *ECCV*, 2020. 1, 2, 6, 7, 10

[7] Yanbei Chen, Shaogang Gong, and Loris Bazzani. Image search with text feedback by visiolinguistic attention learning. In *Proceedings of the IEEE/CVF Conference on Computer Vision and Pattern Recognition*, pages 3001–3011, 2020. 1, 2, 6, 7, 10

[8] Zhao-Min Chen, Xiu-Shen Wei, Peng Wang, and Yanwen Guo. Multi-label image recognition with graph convolutional networks. In *Proceedings of the IEEE/CVF Conference on Computer Vision and Pattern Recognition*, pages 5177–5186, 2019. 2, 5

[9] Ke Cheng, Yifan Zhang, Xiangyu He, Weihan Chen, Jian Cheng, and Hanqing Lu. Skeleton-based action recognition with shift graph convolutional network. In *Proceedings of the IEEE/CVF Conference on Computer Vision and Pattern Recognition*, pages 183–192, 2020. 2

[10] Maxwell Forbes, Christine Kaeser-Chen, Piyush Sharma, and Serge Belongie. Neural naturalist: generating fine-grained image comparisons. *arXiv preprint arXiv:1909.04101*, 2019. 6

[11] Akira Fukui, Dong Huk Park, Daylen Yang, Anna Rohrbach, Trevor Darrell, and Marcus Rohrbach. Multimodal compact bilinear pooling for visual question answering and visual grounding. *arXiv preprint arXiv:1606.01847*, 2016. 1, 2, 6, 7

[12] Yash Goyal, Tejas Khot, Douglas Summers-Stay, Dhruv Batra, and Devi Parikh. Making the v in vqa matter: Elevating the role of image understanding in visual question answering. In *Proceedings of the IEEE Conference on Computer Vision and Pattern Recognition*, pages 6904–6913, 2017. 10, 11

[13] Xiaoxiao Guo, Hui Wu, Yu Cheng, Steven Rennie, Gerald Tesauro, and Rogerio Schmidt Feris. Dialog-based interactive image retrieval. *arXiv preprint arXiv:1805.00145*, 2018. 6

[14] Xiaoxiao Guo, Hui Wu, Yupeng Gao, Steven Rennie, and Rogerio Feris. Fashion iq: A new dataset towards retrieving images by natural language feedback. *arXiv preprint arXiv:1905.12794*, 2019. 2, 5, 6

[15] Kaiming He, Xiangyu Zhang, Shaoqing Ren, and Jian Sun. Deep residual learning for image recognition. In *Proceedings of the IEEE conference on computer vision and pattern recognition*, pages 770–778, 2016. 1, 6

[16] Alexander Hermans, Lucas Beyer, and Bastian Leibe. In defense of the triplet loss for person re-identification. *arXiv preprint arXiv:1703.07737*, 2017. 3

[17] Sepp Hochreiter and Jürgen Schmidhuber. Long short-term memory. *Neural computation*, 9(8):1735–1780, 1997. 6

[18] Surgan Jandial, Ayush Chopra, Pinkesh Badjatiya, Pranit Chawla, Mausoom Sarkar, and Balaji Krishnamurthy. Trace: Transform aggregate and compose visiolinguistic representations for image search with text feedback. *arXiv preprint arXiv:2009.01485*, 2020. 1, 2, 6, 7, 10

[19] Jongseok Kim, Youngjae Yu, Seunghwan Lee, and Gunhee Kim. Cycled compositional learning between images and text. 2

[20] Jin-Hwa Kim, Sang-Woo Lee, Donghyun Kwak, Min-Oh Heo, Jeonghee Kim, Jung-Woo Ha, and Byoung-Tak Zhang. Multimodal residual learning for visual qa. *Advances in neural information processing systems*, 29:361–369, 2016. 6, 7

[21] Jin-Hwa Kim, Kyoung-Woon On, Woosang Lim, Jeonghee Kim, Jung-Woo Ha, and Byoung-Tak Zhang. Hadamard product for low-rank bilinear pooling. *arXiv preprint arXiv:1610.04325*, 2016. 1, 2, 6, 7

[22] Thomas N Kipf and Max Welling. Semi-supervised classification with graph convolutional networks. *arXiv preprint arXiv:1609.02907*, 2016. 2, 4

[23] Chundi Liu, Guangwei Yu, Maksims Volkovs, Cheng Chang, Himanshu Rai, Junwei Ma, and Satya Krishna Gorti. Guided similarity separation for image retrieval. 2019. 2

[24] Zheng Liu, Zidong Jiang, Wei Feng, and Hui Feng. Od-gcn: Object detection boosted by knowledge gcn. In *2020 IEEE International Conference on Multimedia & Expo Workshops (ICMEW)*, pages 1–6. IEEE, 2020. 2

[25] Cewu Lu, Ranjay Krishna, Michael Bernstein, and Li Fei-Fei. Visual relationship detection with language priors. In *European conference on computer vision*, pages 852–869. Springer, 2016. 10, 11

[26] Hyeyoung Noh, Paul Hongseok Seo, and Bohyung Han. Image question answering using convolutional neural network with dynamic parameter prediction. In *Proceedings of the IEEE conference on computer vision and pattern recognition*, pages 30–38, 2016. 6, 7

[27] Jeffrey Pennington, Richard Socher, and Christopher D Manning. Glove: Global vectors for word representation. In *Proceedings of the 2014 conference on empirical methods in natural language processing*, pages 1537–1546, 2014. 6

natural language processing (EMNLP), pages 1532–1543, 2014. 6

- [28] Ethan Perez, Florian Strub, Harm De Vries, Vincent Dumoulin, and Aaron Courville. Film: Visual reasoning with a general conditioning layer. In *Proceedings of the AAAI Conference on Artificial Intelligence*, volume 32, 2018. 6, 7
- [29] Minchul Shin, Yoonjae Cho, and Seongwuk Hong. Fashion-iq 2020 challenge 2nd place team’s solution. *arXiv preprint arXiv:2007.06404*, 2020. 1, 2
- [30] Minchul Shin, Sanghyuk Park, and Taeksoo Kim. Semi-supervised feature-level attribute manipulation for fashion image retrieval. *arXiv preprint arXiv:1907.05007*, 2019. 1
- [31] Jasper Snoek, Hugo Larochelle, and Ryan P Adams. Practical bayesian optimization of machine learning algorithms. *arXiv preprint arXiv:1206.2944*, 2012. 2
- [32] Laurens Van der Maaten and Geoffrey Hinton. Visualizing data using t-sne. *Journal of machine learning research*, 9(11), 2008. 8
- [33] Nam Vo, Lu Jiang, Chen Sun, Kevin Murphy, Li-Jia Li, Li Fei-Fei, and James Hays. Composing text and image for image retrieval—an empirical odyssey. In *Proceedings of the IEEE Conference on Computer Vision and Pattern Recognition*, pages 6439–6448, 2019. 1, 2, 3, 6, 7, 10, 11
- [34] Xin Wei, Ruixuan Yu, and Jian Sun. View-gen: View-based graph convolutional network for 3d shape analysis. In *Proceedings of the IEEE/CVF Conference on Computer Vision and Pattern Recognition*, pages 1850–1859, 2020. 2
- [35] Yuning You, Tianlong Chen, Zhangyang Wang, and Yang Shen. L2-gcn: Layer-wise and learned efficient training of graph convolutional networks. In *Proceedings of the IEEE/CVF Conference on Computer Vision and Pattern Recognition*, pages 2127–2135, 2020. 2
- [36] Youngjae Yu, Seunghwan Lee, Yuncheol Choi, and Gunhee Kim. Curlingnet: Compositional learning between images and text for fashion iq data. *arXiv preprint arXiv:2003.12299*, 2020. 6, 7
- [37] Zhou Yu, Jun Yu, Jianping Fan, and Dacheng Tao. Multi-modal factorized bilinear pooling with co-attention learning for visual question answering. In *Proceedings of the IEEE international conference on computer vision*, pages 1821–1830, 2017. 1, 2, 6, 7
- [38] Zhou Yu, Jun Yu, Chenchao Xiang, Jianping Fan, and Dacheng Tao. Beyond bilinear: Generalized multimodal factorized high-order pooling for visual question answering. *IEEE transactions on neural networks and learning systems*, 29(12):5947–5959, 2018. 1, 2, 6, 7
- [39] Bo Zhao, Jiashi Feng, Xiao Wu, and Shuicheng Yan. Memory-augmented attribute manipulation networks for interactive fashion search. In *Proceedings of the IEEE Conference on Computer Vision and Pattern Recognition*, pages 1520–1528, 2017. 1
- [40] Yida Zhao, Shizhe Chen, Zhihao Zhang, and Qin Jin. Ruc-aim3: Improved tirg model for fashion-iq challenge 2020. 2